

# Local Nanoscale Heating Modulates Single-Asperity Friction

Christian Greiner,<sup>†</sup> Jonathan R. Felts,<sup>‡</sup> Zhenting Dai,<sup>‡</sup> William P. King,<sup>‡</sup> and Robert W. Carpick<sup>\*†</sup>

<sup>†</sup>University of Pennsylvania, Department of Mechanical Engineering and Applied Mechanics, Towne Building, 220 South 33rd Street, Philadelphia, Pennsylvania 19104, United States, and <sup>‡</sup>University of Illinois at Urbana–Champaign, Department of Mechanical Science and Engineering, 242 Mechanical Engineering Building, 1206 W. Green Street, Urbana, Illinois 61801, United States

**ABSTRACT** We demonstrate measurement and control of single-asperity friction by using cantilever probes featuring an in situ solid-state heater. The heater temperature was varied between 25 and 650 °C (tip temperatures from  $25 \pm 2$  to  $120 \pm 20$  °C). Heating caused friction to increase by a factor of 4 in air at  $\sim 30\%$  relative humidity, but in dry nitrogen friction decreased by  $\sim 40\%$ . Higher velocity reduced friction in ambient with no effect in dry nitrogen. These trends are attributed to thermally assisted formation of capillary bridges between the tip and substrate in air, and thermally assisted sliding in dry nitrogen. Real-time friction measurements while modulating the tip temperature revealed an energy barrier for capillary condensation of  $0.40 \pm 0.04$  eV but with slower kinetics compared to isothermal measurements that we attribute to the distinct thermal environment that occurs when heating in real time. Controlling the presence of this nanoscale capillary and the associated control of friction and adhesion offers new opportunities for tip-based nanomanufacturing.

**KEYWORDS** Friction, AFM, silicon, heated probes, velocity, capillary bridges, nanotribology

The temperature dependence of friction affects energy dissipation, wear, and reliability in a multitude of systems, including micro- and nanoelectromechanical systems (MEMS/NEMS), yet scientific understanding is lacking. The complex and ubiquitous nature of tribological processes and the associated dissipation of energy motivates the study of the temperature dependence of friction at the nanoscale.<sup>1–6</sup> When macroscopic objects slide in contact, the interface is not continuous but composed of many asperities. The extremely sharp tip of an atomic force microscope (AFM) enables the study individual nanoscale asperities,<sup>7–10</sup> allowing definitive analysis of the underlying physical processes (Figure 1). For example, determining the activation energies of various kinetic processes in friction requires measurements at different temperatures.<sup>11</sup> Previous studies have investigated the temperature dependence of single asperity friction by controlling the substrate temperature.<sup>1,2,4,5,12–15</sup> Here we introduce a new approach by changing the temperature of the tip itself and demonstrate that new insights are found within this model system. A key advantage is that the tip temperature can be rapidly changed in situ with a time constant below 1 ms.<sup>16</sup> These rapid temperature changes allow experimental time scales  $\sim 10^6$  times faster than previous approaches. Thus, one can rapidly and repeatedly separate the temperature effects from others like tip wear and measure more rapid kinetic pro-

cesses. While ultrahigh vacuum (UHV) conditions are desirable for friction studies by allowing nearly contamination-free surfaces, contacts in most applications never function in UHV but in ambient conditions. Thus, we focus on measurements in humid ambient and dry nitrogen atmospheres to determine the effect of humidity on friction. Silicon substrates are chosen since silicon–silicon contacts are critical for many applications including MEMS and NEMS, where friction and wear are major concerns.

The experiments were performed with silicon AFM probes featuring an in situ solid-state heater<sup>17,18</sup> relying on Joule heating of differently doped parts of the cantilever.<sup>16</sup> An

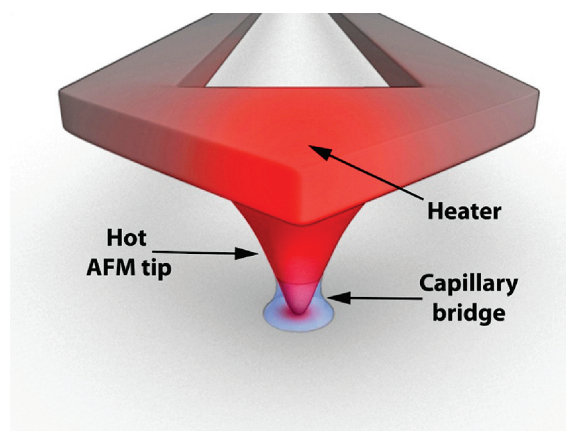


**FIGURE 1.** Schematic of the thermal probe. The heating around the tip–substrate contact is highly localized. In ambient air, a capillary bridge can be nucleated between the tip and substrate. Cantilever heating is achieved through Joule heating of the lower-doped heater region at the end of the cantilever.

\* To whom correspondence should be addressed. E-mail: carpick@seas.upenn.edu.

Received for review: 08/9/2010

Published on Web: 10/07/2010

electric current is driven through the cantilever circuit, which includes the two highly doped legs and the lightly doped heater region, where the tip is located. The higher electrical resistance allows the end of the cantilever to reach temperatures ranging from room temperature (RT) up to approximately 650 °C. The heater temperature was not controlled directly. Instead, constant DC voltages were applied across the cantilever legs via a function generator (Model 33120A, Agilent Technologies, Santa Clara, CA) in combination with a scaling amplifier (Model SIM983, Stanford Research Systems, Sunnyvale, CA or HSA4101, NF Corporation, Yokohama, Japan). Calibration between heater temperature and supplied voltage was performed by micro Raman experiments for each cantilever.<sup>16,19</sup> Silicon (100) wafers with a native oxide layer served as the sample material. The wafers were provided by El-Cat (Waldwick, NJ) and cleaned with piranha solution (5 parts H<sub>2</sub>SO<sub>4</sub>, 1 part H<sub>2</sub>O<sub>2</sub>) to remove all organic contamination. After removal from piranha, the substrates were rinsed with deionized water and blown dry with dry nitrogen. Water contact angle measurements (Ramé-Hart instrument contact angle goniometer, Netcong, NJ) confirmed the extremely hydrophilic nature of the surfaces after piranha cleaning (<5° static contact angle) compared to the as-received Si wafers (37°). The normal force constant of each cantilever was determined in situ at all heater temperatures by applying the reference cantilever method as described by Tortenese et al.<sup>20,21</sup> The reference cantilevers were obtained from Veeco (Santa Barbara, CA). The lateral spring constant of each cantilever was determined with a diamagnetic lateral force calibrator as described by Li et al.,<sup>22</sup> also at each heater temperature. The calibration in lateral and normal direction had to be performed at each heater temperature as normal and lateral spring constants are a function of temperature due to cantilever bending and changes in the elastic modulus of silicon with temperature. With a variation from cantilever to cantilever, they changed by as much as a factor of 3 when heating from room temperature to 650 °C. An Asylum Research (Santa Barbara, CA) MFP-3D AFM was used for all the experiments, except for the pull-off measurements performed in ambient, which were carried out with a Veeco Multimode AFM equipped with a NanoScope IIIa controller. In all experiments, heater temperatures were tested in a randomly alternating order to distinguish effects of temperature from other effects such as tip wear. Air temperature and humidity were continuously monitored (Humidity Meter 11-661-21, Fisher Scientific, Waltham, MA). They were approximately 21 °C and 25–35 % RH respectively for all tests performed in air. For the tests in dry nitrogen, the samples were prepared as described above and placed inside a BioHeater Closed Fluid Cell from Asylum Research. The assembly allowed for a closed confinement that was flushed with dry nitrogen for at least one hour before and during the experiments. While humidity could not be measured during testing, it is expected to be below 3 % RH based on past experiments under similar

conditions. To determine the temperature dependence of friction, experiments were performed at a constant normal load of 112 nN. The scan area was 100 × 100 nm<sup>2</sup>, and the scan rate was 2 Hz for 512 lines. Before starting a scan at this size, a scan for 1 × 1 μm<sup>2</sup> was performed to ensure that the test area was homogeneous and did not give rise to unusual friction signals due to roughness or contamination. Tests were carried out for the unheated state (no applied voltage to the cantilever) and at eight different voltages that corresponded to heater temperatures between approximately 80 and 650 °C at separations of 80 °C in a randomly alternating fashion: 570, 80, 490, 160, 410, 240, 330, and 650 °C. Any twisting and bending of the cantilever with voltage was accounted for by centering the AFM's photodiode at all heater temperatures with the tip retracted from the surface (see Supporting Information Figure S1 for the change in normal and lateral signal due to heating in air and without the tip being in contact). The first and last experiments were performed at room temperature to rule out tip wear influencing the data. As a further check for tip wear, the tip was scanned over an ultrananocrystalline diamond (UNCD) surface before and after each set of experiments.<sup>23</sup> From these scans, the tip reconstruction algorithm of the SPIP software for AFM analysis (ImageMetrology, Hørsholm, Denmark) could be used to estimate the tip shape.<sup>24</sup> It was found that over the course of one set of experiments, there was no detectable change in tip radius. For the experiments with variable normal force, a script was written for the IgorPro software controlling the MFP-3D AFM. This script changed the set point after every scan line, decreasing the load from positive values until the tip pulled off from the sample. As above, the scan consisted of 512 lines across a 100 × 100 nm<sup>2</sup> region at a scan rate of 2 Hz. To investigate the velocity dependence of friction, measurements at 10 different tip velocities ranging from 40 to 7800 nm/s were performed. For these tests, the scan line width was 100 nm, and 128 lines were scanned.

To study the kinetics of capillary condensation in real time, experiments were performed where the heater temperature was increased while scanning for 512 lines at 2 Hz. All these tests started with zero applied voltage to the cantilever. After several scan lines, the voltage was switched on. The heater reached its temperature with a time constant of less than 1 ms.<sup>16,17</sup> After the friction had reached a steady value, the voltage was switched off again. These experiments were performed for all eight heater temperatures in both dry nitrogen and ambient environment. Because of the real-time nature of this method, the twisting and bending of the cantilever could not be corrected for. Because of this, probes were selected that bent upward (away from the sample, thus reducing the applied normal load) upon heating. This ensured that any increase in friction can be attributed to genuine thermal effects and not to an increase in normal load. The effect of cantilever twist was eliminated by calculating friction values as half of the difference between the

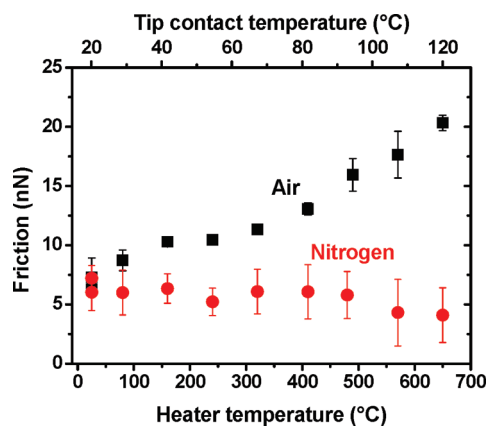


FIGURE 2. Friction as a function of temperature at a constant normal load of 112 nN. Heater temperatures were chosen in a randomly alternating order. Results are from measurements in humid ambient (black squares) and from dry nitrogen (red circles) atmosphere.

lateral trace and retrace signal (friction loop), such that an overall offset in the lateral signal would not affect the measured friction force. All measured data was analyzed using custom MatLab (MathWorks, Natick, MA) code.<sup>25</sup>

In all these experiments, the temperatures at the point of contact between tip and substrate were not known directly. The temperature increase at the contact depends on the tip size and the thermal conductivity ratio of the tip and sample material.<sup>26</sup> Using 20 nm for the tip radius and a thermal conductivity ratio of 1, the temperature increase at the contact is calculated to be approximately 15% of the temperature rise at the heater, based on a detailed thermal model created for this specific thermal probe method.<sup>26</sup> Thus, we estimate that tip temperatures ranged from room temperature to approximately 120 °C. The uncertainty in the temperature rise has many sources including the exact contact pressure and radius, as well as assumptions made in deriving the theory. It is very difficult to give a precise number for the expected error in tip temperature but we conservatively select  $\pm 20$  °C.

Friction forces were measured in both atmospheres as a function of heater temperature (Figure 2). In ambient, as the heater temperature was increased from room temperature to  $\sim 650$  °C, friction at a fixed applied load of 112 nN increased monotonically by a factor of  $\sim 4$ . Using thermal modeling, the tip temperature is estimated to have varied from room temperature to  $120 \pm 20$  °C.<sup>26</sup> In contrast, in dry nitrogen at the same load, the friction forces were slightly smaller, and decreased by  $\sim 40\%$ . Experiments were also conducted with the normal load varied from compressive loads to pull off (the point of adhesive separation under tensile loading) (Figure 3). Again, under ambient conditions friction increased with heater temperature. The adhesive pull-off force  $P_c$  also increased with temperature, as did the slope of the friction-load plots. These trends were absent in dry nitrogen. Individual force-displacement tests reproduced the adhesion trends (Supporting Information Figure S3).

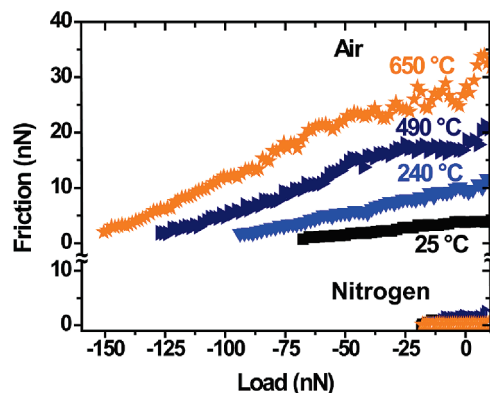


FIGURE 3. Friction as a function of normal load. Friction was measured while the normal force was decreased until the tip pulled off from the substrate. The data for four selected temperatures for humid ambient air and dry nitrogen environment are shown. Note the extended ordinate. The data for all eight heater temperatures can be found in the Supporting Information (Figure S2).

We also performed experiments with tip sliding velocities between 40 and 7800 nm/s (Figure 4). Once more, absolute friction values were lower in dry nitrogen than in air. Furthermore, the trends with velocity are distinct. In ambient, friction decreased with velocity. The trend is more pronounced for higher temperatures, varying by up to a factor of 2. For the four lower temperatures, friction values show a plateau at higher velocities or even a slight increase, with the plateau transition shifting to lower velocities at lower temperatures. In dry nitrogen, there is no dependence on velocity.

All measurements in ambient contradict the common description of frictional slip as a thermally activated sliding process based on the Prandtl–Tomlinson model,<sup>27–30</sup> which predicts friction to decrease with temperature and increase with velocity. However, in dry nitrogen, friction decreased with temperature, and the absolute friction and adhesion values were lower than in ambient. We attribute the influence of humidity on friction and adhesion to the formation of a water meniscus at the tip–sample interface in humid conditions. Experiments<sup>31,32</sup> and Monte Carlo modeling<sup>33–35</sup> demonstrate the existence of capillary condensation at nanoscale tip–sample contacts, and liquid bridges between silicon AFM probes and silicon or gold-coated silicon substrates were directly imaged in environmental scanning electron microscopy (ESEM).<sup>36,37</sup>

We thus explain the modulation of friction with contact temperature as follows: the formation of nanoscale liquid bridges is thermodynamically favored for hydrophilic surfaces at 30% RH at room temperature. While the hydrophilic surface of the sample ought to facilitate the nucleation of the meniscus, the tip itself was not subjected to piranha treatment and is likely to be more hydrophobic. Moreover, capillary formation is a thermally activated process.<sup>14</sup> Higher temperatures help to overcome the activation barrier more rapidly, leading to more fully developed capillaries. This explains the trend of higher friction and adhesion forces with

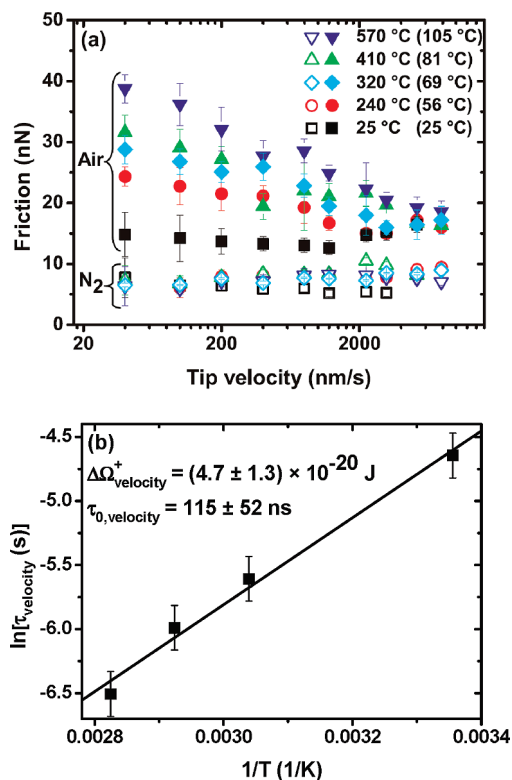


FIGURE 4. Friction as a function of sliding velocity. (a) Friction measurements where the velocity was varied between 40 and 7800 nm/s while the normal load was kept constant at 112 nN. Measurements were performed for five different heater temperatures: room temperature, 240, 320, 410, and 570 °C (estimated tip temperatures: 25, 56, 69, 81, and 105 °C). Open symbols are used for the measurements performed in dry nitrogen, closed symbols for the ones in humid air. (b) Arrhenius analysis of the data presented in (a) by plotting  $\ln(\tau)$  as a function of  $1/T$  where  $T$  is the tip temperature and  $\tau$  the mean capillary nucleation time. The experimental values are fitted with an Arrhenius law yielding the nucleation energy barrier  $\Delta\Omega^+$  and the inverse attempt frequency  $\tau_0$ .

temperature in ambient, as the capillary bridge creates an additional attractive force between tip and sample (due to both the Laplace pressure and the liquid surface tension) and the resulting increased tip–sample contact area increases friction. We expect negligible amounts of water were present in dry nitrogen as the relative humidity is below 3%, inhibiting liquid bridge formation, and so friction decreases with temperature due to thermally activated sliding.<sup>27,28</sup>

The decrease in friction with velocity observed in ambient disagrees with the thermally activated model of friction<sup>29,30</sup> and suggests the following, as first proposed by Riedo et al.:<sup>14,38</sup> at higher velocities, it becomes increasingly difficult for the capillary to follow the sliding contact, as limited by a characteristic critical velocity  $v_c$ . This may result from the capillary encountering defects that pin it to the substrate, or regions of lower topography that break the capillary since it has to stretch to be maintained. Once the capillary is destroyed, there is a barrier to the nucleation of a new capillary. This corresponds to the onset of the plateau region in Figure 4. Assuming that the capillary formation follows

Arrhenius kinetics,<sup>39,40</sup> the formation and the movement of the bridge is thermally activated, so higher heater temperatures shift the plateau's onset to higher velocities. The lack of a decrease in friction with velocity in dry nitrogen (open symbols in Figure 4a) is consistent with this argument. In a highly relevant study, Szoszkiewicz and Riedo<sup>14</sup> measured friction between a silicon tip and soda lime glass at 37% relative humidity from 26 to 59 °C sample temperature, reporting similar behavior. Performing a similar analysis, we extract the critical velocities  $v_c$  at each temperature and from this, the mean capillary nucleation time  $\tau$ .<sup>14</sup> Assuming Arrhenius behavior<sup>39,40</sup> we write  $\tau = \tau_0 \exp[\Delta\Omega^+/k_B T]$  with  $1/\tau_0$  being the attempt frequency and  $\Delta\Omega^+$  the nucleation energy barrier. A linear fit to a plot of  $\ln[\tau]$  versus  $1/T$  (Figure 4b) yields the nucleation energy barrier (slope) and  $\tau_0$  (y-intercept). We find  $\Delta\Omega_{\text{velocity}}^+ = (4.7 \pm 1.3) \times 10^{-20}$  J (0.29 ± 0.08 eV) and  $\tau_{0,\text{velocity}} = 115 \pm 52$  ns. These values resemble those reported in ref 14 and the subsequent erratum:<sup>41</sup>  $\Delta\Omega^+ = (7.8 \pm 0.9) \times 10^{-20}$  J (0.49 ± 0.06 eV) and  $\tau_0 = 126 \pm 122$  ns. As the surface chemistry of the soda lime glass and our silicon wafers with native oxide are similar, this is not unexpected. We note that at even higher temperatures, the capillary is expected to be driven off by evaporation; experiments are underway to examine this regime.

These results and other literature (see Supporting Information) claiming an influence of capillaries on adhesion and friction in AFM, and the importance of AFM for nanotechnology in general, motivates the careful study of the kinetics of capillary condensation. All previous work has been indirect, relying on different sliding velocities or slow variations in temperature<sup>14</sup> by changing the temperature of the entire experimental setup. These indirect methods cannot acquire data in real time and thus are not able to unambiguously determine the order of the kinetic process. Making use of the rapid heating capabilities that thermal probes offer enables a direct in situ approach here. In addition, it allows for a larger temperature range to be investigated than accessible previously. We changed the tip temperature while scanning, ramping from room temperature to eight different tip temperatures (120 °C maximum) and monitored friction in real time (Figure 5a in air, Supporting Information Figure S5 in dry nitrogen). Friction values in Figure 5a are constant at the beginning of the scan and started to increase over time  $t$  when the cantilever was heated due to the formation of the capillary bridge. The friction increase versus time was fitted to an equation of the form  $f(t) = 1 - \exp[t/\tau]$ , where the nucleation time  $\tau$  is the fit parameter (Figure 5a, red line). Plotting  $\ln(\tau)$  versus  $1/T$  (Figure 5b) shows a clear linear trend with an activation energy of  $\Delta\Omega_{\text{in situ}}^+ = (6.4 \pm 0.6) \times 10^{-20}$  J (0.40 ± 0.04 eV) and  $\tau_{0,\text{in situ}} = 9.8 \pm 4.3$  μs. The value for  $\Delta\Omega_{\text{in situ}}^+$  is similar to that from the velocity analysis,  $\Delta\Omega_{\text{velocity}}^+ = (4.7 \pm 1.3) \times 10^{-20}$  J (0.29 ± 0.08 eV), but  $\tau_0$  is nearly 2 orders of magnitude slower than that found using the isothermal measurements as a function of velocity either using a thermal probe (as presented above) or with indirect

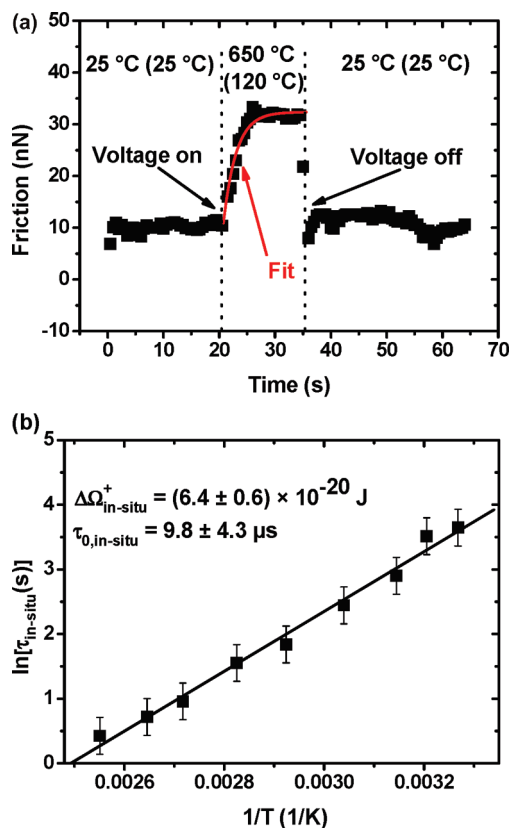


FIGURE 5. Real-time heating experiments in ambient. The temperature of the heater is changed while scanning. In (a) the experiment started with the cantilever being at room temperature. Then the voltage corresponding to a heater temperature of 650 °C (tip temperature is given in parentheses) was switched on. After a steady friction value is reached, the voltage was switched off again. The red line indicates the fit to the data with  $f(t) = 1 - \exp(-t/\tau)$  shifted and normalized to the clearly resolved initial and final friction forces, where  $t$  is the time and  $\tau$  the capillary nucleation time (fit parameter) (b) Arrhenius analysis of the capillary nucleation time  $\tau$  obtained from fitting to the real-time experiments for all eight temperatures. See Supporting Information for all experiments and in both atmospheres.

heating of the entire experiment.<sup>14</sup> This difference seems surprising, but can be explained by the isothermal nature of the velocity analyses versus the changing local temperature for the real-time experiments. For the real-time measurements, the lack of heat in the surrounding environment (which would be present with an indirect method, or during our isothermal velocity measurements<sup>42</sup>) renders the kinetics much slower because of the reduced local partial pressure of water vapor. Thus, the heating method is not just an instrumental issue, but rather, it can completely change the local kinetic conditions. This is a critical issue in considering capillary formation in different environments, including for frictional contacts where the surroundings may be at ambient temperatures but heating from friction at small contact points can be highly localized. Furthermore, the velocity experiments involve interactions with far more sample inhomogeneities. Finally, the fact that an exponential with a single time constant can be used for fitting

the data is significant as it shows that the phenomenon is well-described by first-order kinetics, something that the indirect methods cannot unambiguously determine.

These results also establish that friction is truly a direct probe of the presence of the capillary. We do this by showing here that friction, adhesion, and temperature are all jointly related via the capillary phenomenon as the temperature changes (Figure 3). Previous isobaric measurements<sup>14</sup> have only correlated friction with capillary condensation as the temperature is varied and did not measure adhesion, even though it is known from isothermal studies that variation in partial pressure affects adhesion. Showing the complete correlation between friction and adhesion as a function of temperature (or capillary nucleation) for both dry and humid conditions established that friction is a reliable probe of the presence of a capillary. These results allow us to determine the extent to which friction data are affected by the water meniscus.

The ability to control friction and adhesion, and to nucleate and eliminate a meniscus in situ, creates several new opportunities. Tip-based nanomanufacturing and nanolithography schemes that rely on chemical reactions could be controlled by turning the meniscus on and off, as well as by temperature itself.<sup>45</sup> NEMS/MEMS actuation could be controlled by the substantial, reversible change in friction forces that can be achieved. The results may also be relevant at larger length scales. For example, experiments on granular media reported contact aging behavior that depends on thermally activated menisci.<sup>44</sup> This is relevant to geological systems, where a thorough understanding of friction in fault systems is not established yet.

In summary, we introduced a new way of controlling nanoscale friction by using AFM probes with a solid-state heater. In ambient atmosphere, a thermally activated capillary bridge formed between tip and substrate, increasing friction and adhesion. The capillary's ability to follow the sliding tip is limited, producing a decrease in friction with velocity followed by a plateau. The behavior at various fixed temperatures and during real-time temperature variation follows Arrhenius-like behavior, allowing extraction of the energy barrier and nucleation time for capillary formation. The behavior is suppressed in dry nitrogen. Future experiments will concentrate on using ultrahigh vacuum conditions and substrate materials with a lower thermal conductivity that will increase the temperatures at the contact. These results demonstrate the fascinating potential of the thermal AFM tips to probe phenomena at the nanoscale and also show the ability to control nanoscale friction, adhesion, and capillarity in situ and in real time.

**Acknowledgment.** This research was partially supported by the Nano/Bio Interface Center through the National Science Foundation NSEC DMR08-32802. Acknowledgment is made to the Donors of the American Chemical Society Petroleum Research Fund for partial support of this research as well as to DARPA's program on Tip-Based Nanofabrica-

tion. C.G. acknowledges a Feodor Lynen Fellowship of the Alexander von Humboldt foundation. We thank T. Das and Professor Y. Goldman for assistance with the Asylum AFM and Dr. M. Brukman for help with the variable load experiments. Contact angle measurements were carried out in Professor Shu Yang's group at the University of Pennsylvania.

**Note Added after ASAP Publication.** The caption of Figure 2 was modified in the version of this paper published ASAP October 7, 2010. The correct version published October 25, 2010.

**Supporting Information Available.** Figures S1–S5 and additional discussion. This material is available free of charge via the Internet at <http://pubs.acs.org>.

## REFERENCES AND NOTES

- Schirmeisen, A.; Jansen, L.; Holscher, H.; Fuchs, H. *Appl. Phys. Lett.* **2006**, *88*, 123108.
- Brukman, M. J.; Gao, G. T.; Nemanich, R. J.; Harrison, J. A. *J. Phys. Chem. C* **2008**, *112* (25), 9358–9369.
- Krylov, S. Y.; Frenken, J. W. M. *J. Phys.: Condens. Matter* **2008**, *20* (35), 354003.
- Zhao, X.; Hamilton, M.; Sawyer, W. G.; Perry, S. S. *Tribol. Lett.* **2007**, *27*, 113.
- Zhao, X. Y.; Phillipot, S. R.; Sawyer, W. G.; Sinnott, S. B.; Perry, S. S. *Phys. Rev. Lett.* **2009**, *102* (18), 186102.
- Tshiprut, Z.; Zelner, S.; Urbakh, M. *Phys. Rev. Lett.* **2009**, *102* (13), 136102.
- Binnig, G.; Quate, C. F.; Gerber, C. *Phys. Rev. Lett.* **1986**, *56* (9), 930–933.
- Mate, C. M.; McClelland, G. M.; Erlandsson, R.; Chiang, S. *Phys. Rev. Lett.* **1987**, *59* (17), 1942–1945.
- Carpick, R. W.; Salmeron, M. *Chem. Rev.* **1997**, *97* (4), 1163–1194.
- Szlufarska, I.; Chandross, M.; Carpick, R. W. *J. Phys. D: Appl. Phys.* **2008**, *41* (12), 123001.
- Jacobs, T.; Gotsmann, B.; Lantz, M.; Carpick, R. *Tribol. Lett.* **2010**, *39* (3), 257–271.
- Jansen, L.; Schirmeisen, A.; Hedrick, J. L.; Lantz, M. A.; Knoll, A.; Cannara, R.; Gotsmann, B. *Phys. Rev. Lett.* **2009**, *102* (23), 236101.
- Bao, H. F.; Li, X. X. *Rev. Sci. Instrum.* **2008**, *79* (3), No. 033701.
- Szoszkiewicz, R.; Riedo, E. *Phys. Rev. Lett.* **2005**, *95* (13), 135502.
- Szoszkiewicz, R.; Riedo, E. *Appl. Phys. Lett.* **2005**, *87* (3), No. 033105.
- Lee, J.; Beechem, T.; Wright, T. L.; Nelson, B. A.; Graham, S.; King, W. P. *J. Microelectromech. Syst.* **2006**, *15* (6), 1644–1655.
- Lee, J.; King, W. P. *Sens. Actuators, A* **2007**, *136*, 291–298.
- King, W. P.; Kenny, T. W.; Goodson, K. E.; Cross, G.; Despont, M.; Durig, U.; Rothuizen, H.; Binnig, G. K.; Vettiger, P. *Appl. Phys. Lett.* **2001**, *78* (9), 1300–1302.
- Nelson, B. A.; King, W. P. *Sens. Actuators, A* **2007**, *140*, 51–59.
- Tortonese, M.; Kirk, M. *Proc. SPIE - Int. Soc. Opt. Eng.* **1997**, *3009*, 53–60.
- Ohler, B. *Veeco Calibration Instructions*; Veeco Instruments: Santa Barbara, CA, 2007.
- Li, Q.; Kim, K. S.; Rydberg, A. *Rev. Sci. Instrum.* **2006**, *77* (6), No. 065105.
- Sumant, A. V.; Grierson, D. S.; Gerbi, J. E.; Birrell, J.; Lanke, U. D.; Auciello, O.; Carlisle, J. A.; Carpick, R. W. *Adv. Mater.* **2005**, *17* (8), 1039.
- Villarrubia, J. S. *J. Res. Natl. Inst. Stand. Technol.* **1997**, *102* (4), 425–454.
- Nanoprobe Network*; <http://nanoprobenetwork.org/welcome-to-the-carpick-labs-software-toolbox>. Access date 05/04/2009.
- Nelson, B. A.; King, W. P. *Nanoscale Microscale Thermophys. Eng.* **2008**, *12* (1), 98–115.
- Tomlinson, G. A. *Philos. Mag. Ser.* **1929**, *7* (46), 905–939.
- Prandtl, L. *Z. Angew. Math. Mech.* **1928**, *8* (2), 85.
- Gnecco, E.; Bennewitz, R.; Gyalog, T.; Loppacher, C.; Bammerlin, M.; Meyer, E.; Guntherodt, H. J. *Phys. Rev. Lett.* **2000**, *84* (6), 1172–1175.
- Bennewitz, R.; Gnecco, E.; Gyalog, T.; Meyer, E. *Tribol. Lett.* **2001**, *10* (1–2), 51–56.
- Piner, R. D.; Zhu, J.; Xu, F.; Hong, S. H.; Mirkin, C. A. *Science* **1999**, *283* (5402), 661–663.
- Ginger, D. S.; Zhang, H.; Mirkin, C. A. *Angew. Chem., Int. Ed.* **2004**, *43* (1), 30–45.
- Jang, J.; Schatz, G. C.; Ratner, M. A. *Phys. Rev. Lett.* **2003**, *90* (15), 156104.
- Jang, J. Y.; Schatz, G. C.; Ratner, M. A. *Phys. Rev. Lett.* **2004**, *92* (8), No. 085504.
- Jang, J.; Ratner, M. A.; Schatz, G. C. *J. Phys. Chem. B* **2006**, *110* (2), 659–662.
- Weeks, B. L.; Vaughn, M. W.; DeYoreo, J. J. *Langmuir* **2005**, *21* (18), 8096–8098.
- Weeks, B. L.; DeYoreo, J. J. *J. Phys. Chem. B* **2006**, *110* (21), 10231–10233.
- Riedo, E.; Levy, F.; Brune, H. *Phys. Rev. Lett.* **2002**, *88*, 185505.
- Restagno, F.; Bocquet, L.; Biben, T. *Phys. Rev. Lett.* **2000**, *84* (11), 2433–2436.
- Restagno, F.; Bocquet, L.; Biben, T.; Charlaix, E. *J. Phys.: Condens. Matter* **2000**, *12* (8A), A419–A424.
- Szoszkiewicz, R.; Riedo, E. *Phys. Rev. Lett.* **2007**, *98* (13), 139904.
- The heated region is estimated to span several micrometers from the tip whereas the scanning length is only 100 nm.
- Fletcher, P. C.; Felts, J. R.; Dai, Z.; Jacobs, T. D.; Zeng, H.; Lee, W.; Sheehan, P. E.; Carlisle, J. A.; Carpick, R. W.; King, W. P. *ACS Nano* **2010**, *4* (6), 3338–3344.
- Bocquet, L.; Charlaix, E.; Ciliberto, S.; Crassous, J. *Nature* **1998**, *396* (6713), 735–737.